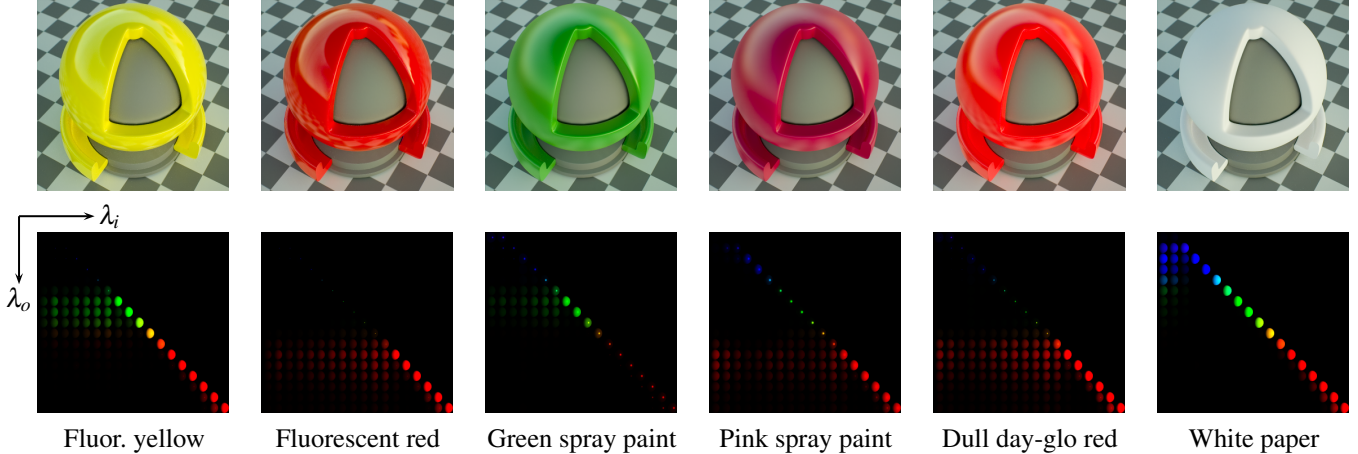


# Acquisition and Analysis of Bispectral Bidirectional Reflectance and Reradiation Distribution Functions

Matthias B. Hullin<sup>1</sup> Johannes Hanika<sup>2</sup> Boris Ajdin<sup>2</sup> Hans-Peter Seidel<sup>1</sup> Jan Kautz<sup>3</sup> Hendrik P. A. Lensch<sup>2</sup>

<sup>1</sup>MPI Informatik      <sup>2</sup>Ulm University      <sup>3</sup>University College London



**Figure 1:** Fluorescent materials absorb part of the incoming light at wavelength  $\lambda_i$  and reradiate it at the longer wavelength  $\lambda_o$ . We have measured bispectral BRRDFs to capture such materials and render them in the spectral environment map of a winter sunset. The bottom row depicts slices of the bispectral BRRDF, showing one rendered sphere for each pair of incident and reflected or reradiated wavelengths  $(\lambda_o, \lambda_i) \in [400\text{nm}; 720\text{nm}] \times [380\text{nm}; 720\text{nm}]$ . Fluorescence is represented by the off-diagonal entries.

## Abstract

In fluorescent materials, light from a certain band of incident wavelengths is reradiated at longer wavelengths, i.e., with a reduced per-photon energy. While fluorescent materials are common in everyday life, they have received little attention in computer graphics. Especially, no bidirectional reradiation measurements of fluorescent materials have been available so far. In this paper, we extend the well-known concept of the bidirectional reflectance distribution function (BRDF) to account for energy transfer between wavelengths, resulting in a *Bispectral Bidirectional Reflectance and Reradiation Distribution Function* (bispectral BRRDF). Using a bidirectional and bispectral measurement setup, we acquire reflectance and reradiation data of a variety of fluorescent materials, including vehicle paints, paper and fabric, and compare their renderings with RGB, RGB  $\times$  RGB, and spectral BRDFs. Our acquisition is guided by a principal component analysis on complete bispectral data taken under a sparse set of angles. We show that in order to faithfully reproduce the full bispectral information for all other angles, only a very small number of wavelength pairs needs to be measured at a high angular resolution.

**CR Categories:** I.4.1 [Image Processing and Computer Vision]: Digitization and Image Capture—Reflectance;

I.3.7 [Computer Graphics]: Three-Dimensional Graphics and Realism—Color, shading, shadowing, and texture;

**Keywords:** fluorescence, spectral BRDF, bispectral BRRDF, bispectral rendering

## 1 Introduction

Fluorescent materials change the wavelength of light upon reflection. This applies to many everyday materials, for instance human

teeth, utility vehicle paints, detergents (fabric whiteners), or even ordinary photocopying paper. This shift of wavelength causes compelling visual effects if it occurs within the visible spectrum or turns UV radiation into visible light. In particular, many fluorescent surfaces appear brighter than perfectly white surfaces (Figure 2).

The underlying physical mechanism is well understood. A fluorescent medium consists of atoms or molecules that absorb incident photons at a given wavelength, and re-emit them after a short time (in the order of  $10^{-8}\text{s}$ ). During this time interval, the electrons of the fluorescent molecule remain in an excited state above the ground energy level. The re-emission of a photon occurs as the fluorophore relaxes to its ground state. Due to mechanical interaction with the surrounding molecules, some of the excitation energy is lost during this process, leading to a change of wavelength, or Stokes shift. As required for conservation of energy, except in the case of multi-photon interactions, this shift always occurs towards longer wavelengths, corresponding to a loss in per-photon energy.

The wavelength-shifting behavior of a fluorescent material can be intuitively described *bispectrally* using a so-called *reradiation matrix* [Donaldson 1954], specifying for each combination of incoming and outgoing wavelengths the amount of reradiated light. At



**Figure 2:** Spheres covered in three different multilayer paint varieties for utility vehicles (“pearl white” primer, fluorescent red/yellow/orange paint, clear coat). Note the outstanding chroma of the paints, and their luminance, which even in the non-specular part is higher than the one of the 90% white ColorChecker patch.

the same time, however, the reflectance of every real-world material also depends on the directions of the incident and reflected light rays with regard to the surface, as usually described by the *bidirectional reflectance distribution function* (BRDF) [Nicodemus et al. 1977]. In this paper, we integrate these well-known concepts into the *bispectral BRRDF*<sup>1</sup> that can describe general fluorescent (and non-fluorescent) materials and the bidirectional dependency of their wavelength-preserving reflectance and their wavelength-shifting reradiation.

While there have been attempts to approximate fluorescent materials with analytical models, to our knowledge the full bidirectional and bispectral reflectance of real materials has not been measured so far. By equipping a traditional BRDF measurement setup with spectral filters for light source and camera, we acquire bispectral BRRDF datasets for a range of isotropic fluorescent materials.

Given the measured data, we project them into a sparse spectral basis using principal component analysis (PCA). Such a decomposition, when performed on a partially acquired dataset, allows for efficient planning of the remaining acquisition task.

## 2 Related Work

**Analytical and data-based BRDF models.** The history of data-based BRDF models in the context of computer graphics goes back to the early nineties, when Ward [1992] measured and modeled the BRDF of anisotropic materials. The first larger material database of 61 different, albeit sparsely sampled BRDFs emanated from the CUReT project [1996]. Later on, Matusik et al. [2003a] measured more than 100 different materials (similar setup to Marschner et al. [2000]), from which they derived a generative BRDF model. Ngan et al. [2005] compiled an overview of different models and how well they approximate BRDF measurements. Many of these BRDF models allow for spectrally varying reflectance distributions, such as the Cook-Torrance BRDF [Cook and Torrance 1981], but do not model bispectral distributions as needed for the reproduction of fluorescence.

**Color characterization and reproduction.** It is widely acknowledged that the reproduction of colors benefits from spectral treat-

<sup>1</sup>In optics, the *bispectral luminescent radiance factor* is commonly used to describe fluorescent materials. This is inconvenient for our purposes, as it defines fluorescence relative to a perfect, non-fluorescent diffuser.

Note that reflection and reradiation are different physical mechanisms and are treated as such throughout the scientific literature. In a computer graphics context, however, it makes sense to abstract reradiation as an instantaneous phenomenon and treat it in the same way as reflectance.

ment above the usual red, green, blue (RGB) channels. A very comprehensive treatment of many questions within the field of color science was given by Nassau [1983]. More within the field of reflectance capture, [Proctor and Barnes 1996] constructed a spectral BRDF measuring gantry featuring a tunable monochromatized light source and broadband receiver, which makes it suitable for spectral, but not for bispectral measurements.

**Bispectral measurement.** Within the field of fluorometry, bispectral measurements are a long-established technique [Leland et al. 1997]. In fact, the concept of a reradiation matrix dates back over half a century [Donaldson 1954]. Due to the high dimensionality of the reflectance and reradiation function, researchers usually put more focus on the spectral dimension and constrained themselves to very sparse angular sampling of BRDFs, typically at  $0^\circ/45^\circ$  or  $0^\circ/10^\circ$  when performing spectral or bispectral measurements [Angelopoulou and Molana 2001; Gundlach and Terstiege 1994; Hersch et al. 2007]. In order to vary between these angular settings Holopainen et al. [2008] proposed a carefully calibrated bispectral goniometer setup, but the limited angular range and resolution prevents sampling a full BRRDF.

**Rendering of fluorescence.** [Glassner 1994] was the first to adapt the rendering equation [Kajiya 1986] to include fluorescence (as well as phosphorescence). Within the field of computer graphics, the next significant step was taken by [Wilkie et al. 2001], who introduced a rendering framework that is capable of treating polarization and fluorescence effects in a joint fashion. More recently, Wilkie et al. went on to derive a physically motivated multilayer reflectance model that allows for the inclusion of fluorophores in the diffuse layer [2006]. In this work, they also performed a qualitative analysis of a fluorescent material, optimizing their model parameters to visually match the reflection of a green laser on an orange fluorescent cardboard. The authors conclude that while fluorescence is mostly a diffuse effect, it may still depend on the view/light directions, e.g., due to additional Fresnel effects.

In this work, our goal is not the derivation of parameters for an analytical model. Rather, we demonstrate how it is possible in a data-driven setting to acquire real-world reflectance data efficiently by taking into account the complexity of the given material.

## 3 Bispectral Reflectance and Reradiation

For computer graphics purposes the phenomena of reradiation and reflection can be treated in an unified manner, albeit being physically different. We will henceforth refer to both phenomena as “bispectral reflectance” while keeping our terminology as compatible as possible with the metrology and physics literature.

### 3.1 Bispectral Rendering Equation

Light transport considering energy transfer from one wavelength to another, in order to account for fluorescence, can be expressed by the bispectral rendering equation:

$$L(\omega_o, \lambda_o) = L_e(\omega_o, \lambda_o) + \int_{\Omega} \int_{\Lambda} L(\omega_i, \lambda_i) f_r(\omega_o, \omega_i, \lambda_o, \lambda_i) \cos\theta d\lambda_i d\omega_i, \quad (1)$$

which in contrast to the standard rendering equation [Kajiya 1986] requires an additional integration over all incident wavelengths  $\lambda_i$ . In order to stay consistent with Glassner [1994], we denote the wavelengths by  $\lambda_o$  and  $\lambda_i$  (as opposed to  $\lambda$  and  $\mu$  that are often used in optics and other engineering fields).

Solving the bispectral rendering equation is straightforward when using spectral path tracing, e.g. [Bendig et al. 2008], but of course other rendering techniques can be adopted as well.

|                     |  |  |
|---------------------|--|--|
| Radiance            | $L(\omega)$  | $\left[ \frac{\text{W}}{\text{sr} \cdot \text{m}^2} \right]$                 |
| Spectral Radiance   | $L(\omega, \lambda)$   | $\left[ \frac{\text{W}}{\text{sr} \cdot \text{m}^2 \cdot \text{nm}} \right]$ |
| Spectral Irradiance | $E(\lambda) = \int_{\Omega} L(\omega, \lambda) d\omega$                | $\left[ \frac{\text{W}}{\text{m}^2 \cdot \text{nm}} \right]$                 |
| Irradiance          | $E = \int_{\Lambda} \int_{\Omega} L(\omega, \lambda) d\omega d\lambda$ | $\left[ \frac{\text{W}}{\text{m}^2} \right]$                                 |

**Table 1:** Definitions of spectral quantities;  $\omega$  refers to directions and  $\lambda$  to wavelengths.

### 3.2 Bispectral BRRDF

The bispectral rendering equation includes the *bispectral BRRDF*  $f_r(\omega_o, \omega_i, \lambda_o, \lambda_i)$  that describes the angularly dependent reflectance for any pair of wavelengths. Its definition is different from the well-known definition of a spectral BRDF [Nicodemus et al. 1977] which cannot represent fluorescent materials. Furthermore, it is more general than the use of directionally independent reradiation matrices as proposed by Donaldson [1954].

Before we provide the general bispectral BRRDF, let us briefly recall the definition of a spectral BRDF. The required spectral quantities are defined in Table 1. Note that the spectral quantities feature a different unit compared to their non-spectral counterparts. Following Nicodemus et al. [1977], the differential reflected spectral radiance  $dL_o(\omega_o, \lambda_o)$  due to the incident differential spectral irradiance  $dE(\lambda)$  from direction  $\omega_i$  is given as:

$$dL_o(\omega_o, \lambda) = dE(\lambda) f_r(\omega_o, \omega_i, \lambda) \left[ \frac{\text{W}}{\text{sr} \cdot \text{m}^2 \cdot \text{nm}} \right], \quad (2)$$

with  $\omega_i$  and  $\omega_o$  being the incident and outgoing directions. The spectral BRDF  $f_r(\omega_o, \omega_i, \lambda)$  for a single wavelength is therefore defined as the ratio of differential reflected spectral radiance to differential incident spectral irradiance:

$$f_r(\omega_o, \omega_i, \lambda) = \frac{dL_o(\omega_o, \lambda)}{dE(\lambda)} = \frac{dL_o(\omega_o, \lambda)}{L_i(\omega_i, \lambda) \cos(\theta_i) d\omega_i} \left[ \frac{1}{\text{sr}} \right]. \quad (3)$$

It follows that the unit of the spectral BRDF is  $\left[ \frac{1}{\text{sr}} \right]$ , which is the same as for non-wavelength dependent BRDFs  $f_r(\omega_o, \omega_i)$ , although the units for  $L$  and  $E$  differ in the spectral vs. non-spectral case.

We now generalize Nicodemus' derivation of the BRDF to account for cross-wavelength energy transfer by the bispectral BRRDF and show that its unit differs from the spectral BRDF. Referring to the bispectral rendering equation (Eq. 1) the differential reflected and reradiated spectral radiance (differential with regard to the incident direction  $\omega_i$  and the incident wavelength  $\lambda_i$ ) is due to incident double differential (*non-spectral*) irradiance for  $\omega_i$  and  $\lambda_i$ :

$$d^2L_o(\omega_o, \lambda_o) = d^2E \cdot f_r(\omega_o, \omega_i, \lambda_o, \lambda_i) \left[ \frac{\text{W}}{\text{sr} \cdot \text{m}^2 \cdot \text{nm}} \right], \quad (4)$$

and hence the *bispectral BRRDF* may be defined as

$$f_r(\omega_o, \omega_i, \lambda_o, \lambda_i) = \frac{d^2L_o(\omega_o, \lambda_o)}{L_i(\omega_i, \lambda_i) \cos(\theta_i) d\omega_i d\lambda_i} \left[ \frac{1}{\text{sr} \cdot \text{nm}} \right]. \quad (5)$$

The bispectral BRRDF is a general way to represent fluorescent materials as it does not make any assumptions about the material.

In the discretized case, an individual sample of the bispectral BRRDF for the directions  $(\omega_i, \omega_o)$  expresses the energy transfer from the incoming spectrum to the reflected spectrum as a matrix over  $\lambda_o$  and  $\lambda_i$ , see Figure 1. While the diagonal entries refer to reflection at the same wavelength, the fluorescent effect is represented by the off-diagonal part. As there is typically no transfer from longer to shorter wavelengths (towards higher energy), the upper triangle will remain black.

## 4 Measurement and Reconstruction

### 4.1 Setup

In order to acquire isotropic bispectral BRRDFs, we have built a fully automated image-based measurement device. It follows the design of Matusik et al. [2003a] for isotropic BRDFs but with the added capability to emit and acquire at specific wavelength bands (Figure 3).

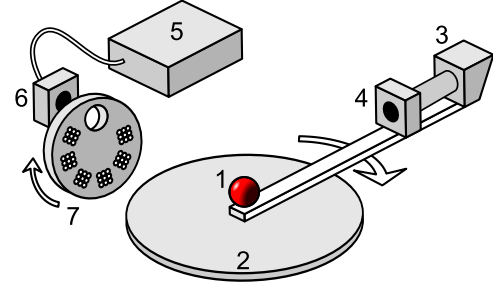


**Figure 3:** A depiction of our setup. A sample sphere (1) is mounted on a turntable (2), to which a digital monochrome still camera (3) is attached. The camera is equipped with a visible-spectrum tunable filter (4). The sphere is illuminated by a light guide coupled xenon light source (5) with another tunable filter (6) mounted in front; near-UV light is generated with LEDs that can be selected using a motorized wheel (7). On the exit aperture of (6) and the entry aperture of (4), we attach optical depolarizers.

The spectral filters used are LCD-based Lyot filters (CRi VariSpec VIS10/35 mm) whose transmission bands are about 10 nm–20 nm wide and range from 400 nm to 720 nm. We apply additional polarization scrambling optics to undo the linear polarization from the LCD filters so as not to bake any unwanted side effects into the measured BRRDF. Figure 4 illustrates the strong influence of polarization both on the specular and the diffuse reflection for a sample with clear coat. Our experiments show that even non-coated, apparently diffuse surfaces do not necessarily completely decorrelate the polarization state.

As light source we employ a xenon arc lamp coupled into a light fiber (XION medical Xenon R180), whose light has a flat and stable spectrum (measured using a spectroradiometer) but rather weak blue and UV output, especially after passing the spectral filter. We therefore add LEDs for better coverage of this range (370 nm–420 nm in 10 nm steps). The camera is a monochrome, digital still camera (Jenoptik ProgRes MFcool), with which we acquire high-dynamic-range images using exposure series from 1 ms to 16 s.

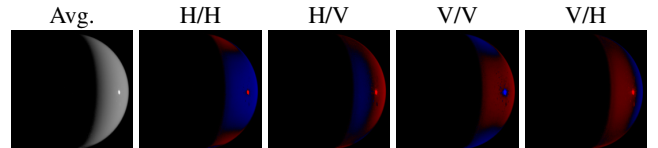


**Figure 4:** Influence of polarization on reflection from a sphere: Average image and difference images (red: negative) depending on the polarization state of light source and observer, where “H/V” stands for “horizontal in, vertical out”. Near the Brewster angle, the specular highlight is contained almost exclusively in the V/V component. Also, note the variation in the diffuse regions.

## 4.2 Geometric and Spectral Calibration

Calibrating such a measurement setup geometrically and spectrally is not a trivial task. On the geometrical side, Havran et al. [2005] propose Helmholtz reciprocity as a validity criterion for the measurement setup. However, luminescent materials (that do not preserve the wavelength of light) do not fulfill Helmholtz reciprocity by nature [Springsteen 1999; Clarke and Parry 1985]. Therefore, we chose to treat the spectral and geometric calibration independently of each other. Geometric validation of our BRRDF measurement setup is provided by a reciprocity check using a non-fluorescent sample sphere.

The spectral response of the system is determined by taking into account the spectral transmission or sensitivity curves for all of the components [DeRose et al. 2007; Holopainen et al. 2008], either as obtained from the manufacturers or calibrated using a photospectrometer. We obtain the absolute scaling from a bispectral measurement on a flat Spectralon target, which preserves the wavelength and has a well-defined reflectance (99% quasi-Lambertian reflectivity across the spectrum). Due to a slight crosstalk between neighboring filter bands, we observe a small contribution of the wavelength-preserving reflection to non-diagonal elements in the bispectral matrix. For normalization, we require the rows of the captured bispectral Spectralon BRRDF sample to add up to  $0.99 \text{ sr}^{-1}$ , which, along with the transmission curves for the illumination and detection branch, gives us a spectral scaling factor  $s(\lambda_o, \lambda_i)$  for each wavelength pair. Any captured camera value is scaled according to  $s(\lambda_o, \lambda_i)$  before generating one entry in the matrix of a bispectral BRRDF sample.

## 4.3 Measurement and Data Processing

The straightforward way of acquiring a bispectral BRRDF is to capture images at all turntable rotations  $\beta$  for every pair of wavelengths  $(\lambda_o, \lambda_i)$ . For practical reasons we constrain ourselves to 20 nm steps in the range from 380 nm to 720 nm for  $\lambda_i$  and 400 nm to 720 nm for  $\lambda_o$ , amounting to 170 images per  $\beta$  as the upper triangle of the bispectral matrix can be ignored. We vary  $\beta$  in the range of  $5^\circ$  to  $170^\circ$ . For highly specular materials a stepping of  $5^\circ$  is chosen to sufficiently sample the sharp highlight while we take a coarser sampling of  $10^\circ$  for materials of lesser angular bandwidth. The acquired data then undergo geometric processing and resampling.

**Adaptive measurement.** In the case of a PCA-steered measurement (Section 5), we first acquire full bispectral data sets for a small number of turntable angles. After performing the PCA decomposition, we acquire dense angular data only for the sparse bispectral basis that is required for a good reconstruction. Only a small set of wavelength pairs needs to be measured.

**Geometric processing.** Depending on the material, we use two different sample geometries: coated spheres for the paints and a custom-made piecewise cylindrical object (Figure 12) wrapped in stripes of paper or fabric.

Due to the varying normals of the shapes each surface point will be illuminated and viewed from a slightly different direction. From simple geometric considerations we can determine  $(\omega_o, \omega_i)$  for every pixel captured under a specific turntable rotation  $\beta$ .

For storage and further processing, we discretize the data for each wavelength pair in  $32^3$  bins using the  $(\theta_o, \theta_i, \phi_{\text{diff}})$  parameterization chosen in [Matusik et al. 2003a]. For the strongly specular materials,  $64^3$  bins are used. Bins that are not populated due to the coarse sampling of the turntable position are filled in by diffusion.

In the rendering step, a specific reflectance sample  $f_r(\theta_o, \theta_i, \phi_{\text{diff}}, \lambda_o, \lambda_i)$  is obtained by multilinear interpolation from our bispectral BRRDF representation.

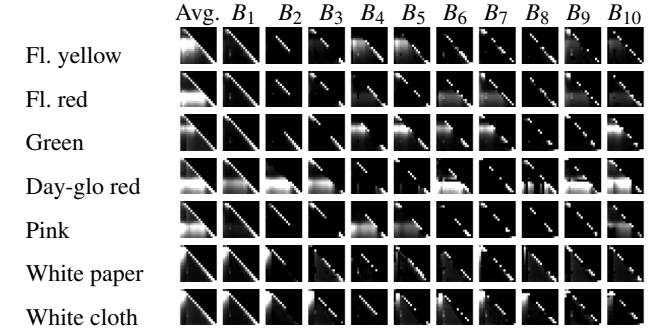


Figure 5: Average and the first 10 principal components  $B_i$ .

## 5 PCA-based Acquisition

In this work, we opt for a data-driven representation of the bispectral BRRDF because we do not want to make strong *a priori* assumptions about the spectral and angular behavior of the material. Particularly, we know that due to the different nature of fluorescent reradiation and specular reflection, the overall spectral and angular variation of most bispectral BRRDFs (say, a diffuse red material with a white highlight) is not strictly separable in the form

$$f_r(\omega_o, \omega_i, \lambda_o, \lambda_i) = f^\lambda(\lambda_o, \lambda_i) f^\omega(\omega_o, \omega_i) \quad (6)$$

This is unfortunate, since it would have allowed us to measure angular and spectral dependencies  $f^\omega$  and  $f^\lambda$  separately and simply compute the bispectral BRRDF as the outer product of both functions. On the other hand, it is always possible to expand  $f_r$  into a series of separable terms:

$$f_r(\omega_o, \omega_i, \lambda_o, \lambda_i) = \sum_n f_n^\lambda(\lambda_o, \lambda_i) f_n^\omega(\omega_o, \omega_i) \quad (7)$$

Since fluorescence, due to its physical nature, is only weakly directional, a PCA will yield such a decomposition of low rank. We exploit this insight and perform a dense bispectral measurement under only a sparse set of turntable angles ( $0^\circ$ ,  $70^\circ$  and  $150^\circ$ , each of which corresponds to a 2D slice of the BRDF). The measurements from this sparse set of turntable positions contain samples from a lot of different angles of incidence and exitance. The bispectral correlations found in these measurements can then be transferred to other angles. Figure 10 illustrates this for measurements taken at two turntable positions.

We assemble a matrix  $F$  which contains all bispectrally-valued BRRDF samples with the average value  $\bar{f}$  subtracted, and compute its SVD. Selecting the  $n$  eigenvectors with the greatest eigenvalues the basis  $B$  is assembled. Examples of such eigenvectors can be seen in Figure 5.

**Measurement basis.** Since our narrowband filter assembly only allows for the sampling of wavelength pairs  $(\lambda_o, \lambda_i)_k$ , we cannot measure in the PCA basis directly. The estimation of a bispectral sample  $f$  from the sparse measurement  $f' = \{f_k(\lambda_o, \lambda_i)\}$  calls for a basis transformation  $P^+$ , which we obtain as the pseudo-inverse of the matrix  $P$  which in turn is composed of the subset of rows of  $B$  corresponding to  $(\lambda_o, \lambda_i)_k$ :

$$f \approx BP^+(f' - \bar{f}) + \bar{f}. \quad (8)$$

The selection of suitable wavelength pairs  $(\lambda_o, \lambda_i)_k$  influences the stability of the approximation which is correlated to the condition number of  $P$ . Starting with the wavelength pair corresponding to the greatest entry in  $B$ , we follow a greedy strategy selecting the set which brings  $\text{cond}(P)$  closest to 1. Our approach is inspired by Matusik et al. [2003b] who reduced the number of measured directional samples for ordinary BRDFs using a similar analysis.

| #Comp.   | 1 | 2 | 3 | 4 | 5 | 10 | 20 | 30 | 1% | 0.1% |
|----------|---|---|---|---|---|----|----|----|----|------|
| Dull red |   |   |   |   |   |    |    |    | 2  | 5    |
| Orange   |   |   |   |   |   |    |    |    | 4  | 7    |
| Green    |   |   |   |   |   |    |    |    | 2  | 6    |
| Pink     |   |   |   |   |   |    |    |    | 2  | 7    |
| Speckled |   |   |   |   |   |    |    |    | 4  | 8    |

**Figure 6:** Image-based same-angle reconstruction of full bispectral data (20 nm resolution) from a small number of acquired bispectral samples. As a reference, we provide ground truth in the top half of each image, and the number of basis vectors required for the residual energy to drop below 1% and 0.1%, respectively. Note that in the case of strong specular highlights (Orange, Speckled), the numerical error does not reflect the visual difference well.

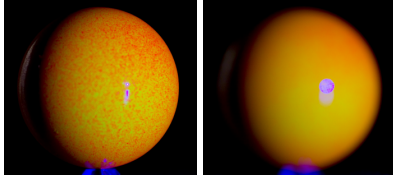


**Figure 7:** The Speckled sample, while not a homogeneous BRRDF, represents the class of mixed materials with angularly dependent visibility of the individual components. Note the red shift towards grazing angles in the defocused shot (right). Photos taken under 420nm light.

## 5.1 Insights

**Same-angle reconstruction using standard PCA.** In Figure 6, we show a reconstruction of a single-angle bispectral measurement from the PCA basis for the same angle. The error measure provided is given by the residual energy as determined by the SVD and relates to the full bispectral dataset with 170 wavelength pairs, not just the resulting sRGB color vectors as shown in the figure. Although the fidelity increases with the cardinality of the measurement basis, the visual appearance even at a numerical error as low as 1% or 0.1% is not always fully satisfactory. It is due to the least-squares nature of the SVD that materials with particularly strong specular highlights (Orange, Speckled) attract the attention of the first few eigenvectors at the expense of a slower convergence in the nonspecular regions. Remarkably, a decent reconstruction is often achieved even before the inclusion of the first measurement of an off-diagonal wavelength pair. In all five examples, the first 9 components were based purely on wavelength-preserving measurements.

**Speckled dataset.** The “Speckled” material (Figure 7) is a fluorescent yellow sphere onto which we manually applied a non-uniform layer of red speckles. While this sample does not have a homogeneous BRRDF, we included it as it represents a material with complex microstructure resulting in directionally dependent fluorescence, as can be seen in the defocused image (Figure 7 right).

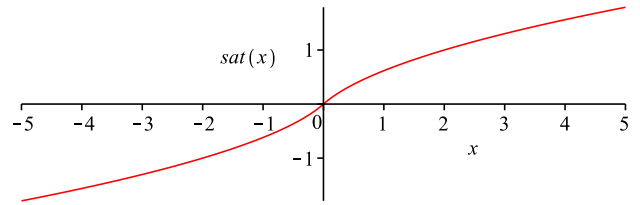


**Figure 8:** As saturation function  $\tilde{x} = \text{sat}(x)$ , we chose the inverse of  $x = \text{sign}(\tilde{x})(\tilde{x}^2 + |\tilde{x}|)$ , which is linear for small values of  $|x|$ , but of  $\mathcal{O}(\sqrt{|x|})$  asymptotically.

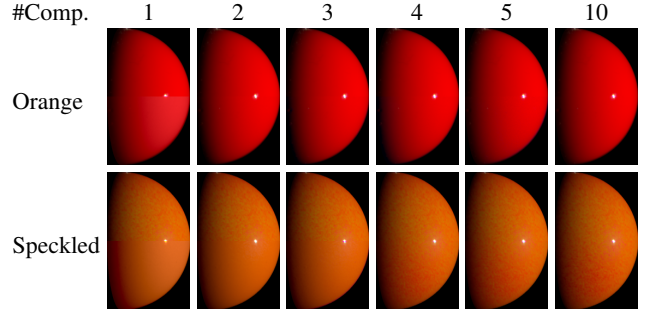


**Figure 9:** By applying a saturation function on the covariance matrix, the convergence in the non-specular parts is significantly improved.

**Taming the specular highlight.** It is to be expected that a signal decomposition based on a  $L^1$  measure would no longer overemphasize the importance of the specular highlight. However, the few  $L^1$ -PCA approaches in existence are computationally rather expensive and, due to their nonlinear optimization scheme, offer no guarantee of global convergence [Baccini et al. 1996; Ke and Kanade 2003]. In order to emulate a similar behavior using a standard PCA, we apply a saturation function on the values in the covariance matrix (and its inverse after the reconstruction), which dampens the high pixel values in the highlight region (Figure 8). As a consequence, the visual convergence is sped up considerably (Figure 9).

**Angular dependency.** For most materials (except Speckled), the resulting principal components show that the fluorescent entries in the reradiation matrix  $\lambda_i \neq \lambda_o$ , taken for themselves, carry a rather weak angular dependency, i.e., indicating reasonable separability. However, as soon as the full matrix, the full bispectral BRRDF including the non-fluorescent elements, is considered, at least two, most often even more separable functions are required for faithful reproduction.

**Angle transfer.** Earlier on, we assumed that the bispectral decomposition of an angular BRRDF slice can be transferred to the spectrally sparse measurements taken under different angles. In Figure 10, we provide experimental evidence for this assumption. Using a PCA basis that was computed using fully-bispectral measurements at turntable angles of  $0^\circ$  and  $70^\circ$ , we reconstruct a fully bispectral intermediate slice at  $35^\circ$  out of only five measured wavelength pairs.

Our PCA-guided measurement routine allows us to drastically reduce the acquisition cost. As an example, let us assume a sampling of  $5^\circ$  steps from  $0^\circ$  to  $150^\circ$  for the turntable position. If all 170 bispectral entries are captured for each angle, the total time of optical exposure amounts to approx. 45 hours. By performing the full bispectral measurement under three turntable orientations only, and by measuring only 5 out of 170 wavelength pairs for the remaining angles, the acquisition time drops to 5.5 hours.

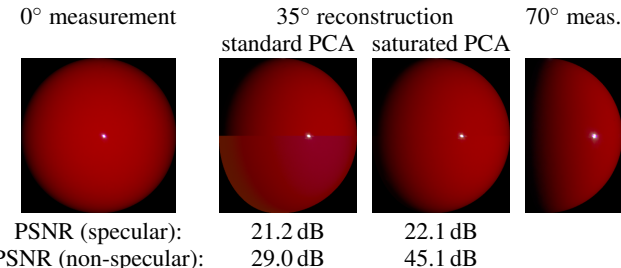


**Figure 10:** Reconstruction of an intermediate angle, which was not sampled for the PCA, from 5 wavelength pairs using the standard and saturated PCA approaches. Again, the top half of the reconstructed images is ground truth. The PSNR has been computed separately for the highlight area and the rest.

## 6 Results

### 6.1 Acquired Datasets

Using our measurement device and acquisition scheme, we have captured bispectral BRRDFs of a number of fluorescent materials, including fluorescent paints with or without clear coating as well as paper and white cloth. As shown in Figure 1, they all have different wavelength ranges for excitation and emission.

The strength of the reradiation therefore depends heavily on the illuminating spectrum as demonstrated in Figure 11 and Figure 12. In Figure 12, RGB photographs are compared against renderings under a 5600K illuminant. As our illumination system contains near-UV LEDs, we can even capture materials such as the paper sample which exhibit significant reradiation in the blue to UV range. The effect is clearly visible in Figure 11. Our captured bispectral BRRDFs faithfully reproduce the fluorescence in both images.

### 6.2 Spectral Detail Level

In Figure 14, we demonstrate that fluorescence does in fact require bispectral modeling of sufficient resolution. After reducing the measured bispectral BRRDF samples to a  $3 \times 3$  (RGB  $\times$  RGB) matrix by integrating over the RGB spectral curves, the renderings show clear differences to the full bispectral BRRDFs. Especially for the Yellow sample, the coarse RGB  $\times$  RGB representation is unable to reproduce reradiation, which is sharply centered around 540 nm. We also integrate the bispectral BRRDF into a spectral BRDF by assuming a uniform illuminant spectrum. Again, the differences can clearly be seen. While they are less pronounced because the illumination in this scene is similar to the spectrum used for the conversion, slight deviations in color and intensity can still be made out. Reducing the bispectral BRRDF to a simple RGB BRDF (again assuming a uniform incident spectrum) shows obvious differences. These differences are most pronounced for non-white spectra as demonstrated in Figure 13.

## 7 Conclusion

Fluorescent materials transfer energy across different wavelength bands. We have provided the definition of the bispectral BRRDF, which enables us to model directionally-dependent fluorescent behavior. The proposed image-based measurement setup can acquire such bispectral reflectance and reradiation functions efficiently.

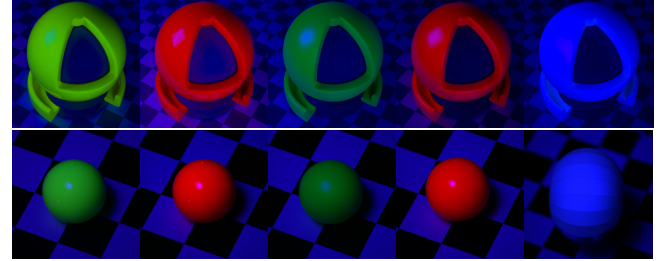
Even though real-world BRRDFs are not directly separable into spectral and angular functions, we can apply a PCA-steered acquisition scheme that only measures relevant bispectral samples of the BRRDF, resulting in a significant speedup (approx. 9:1), rendering such acquisition practical.

One of the shortcomings of a standard PCA in this context is its optimization of an  $L^2$  error function. As a consequence, the importance of specular highlights is often overemphasized, which leads to slower convergence in the non-specular regions. While a  $L^1$ -based decomposition could potentially resolve this issue, we reached a simpler solution that is just as effective. By reweighting the covariance matrix before performing the SVD, we are able to improve the reconstruction fidelity for very small numbers of measured components. This also extends to spatially varying materials. For most of our materials, we can reach a visually indistinguishable reconstruction using only 5 or even fewer measurements per angle (as compared to 3 for a standard RGB measurement). This should allow for efficient acquisition of even higher-dimensional functions (anisotropic bispectral BRRDFs, bispectral BTFs or reflectance fields) in the future.

As another extension to our measurement setup, we currently investigate the possibility of replacing the narrowband tunable spectral filters with hyperspectral devices. Measurements could then be directly performed using bi-hyperspectral basis vectors rather than individual wavelength pairs. The resulting optical path would have a higher overall transmission, which would lead to faster exposure times and/or better noise figures. Furthermore, bi-hyperspectral measurements would allow for more advanced computational sensing approaches such as multiplexed illumination or compressed sensing.

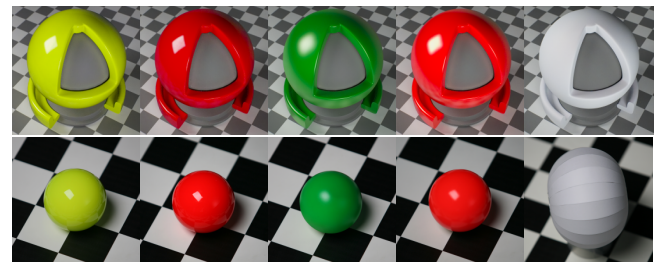
### Acknowledgements

Our thanks go to Ivo Ihrke, Karol Myszkowski and Michael Wand, as well as the anonymous reviewers for many useful comments and suggestions. This work was partially funded by a DFG Emmy Noether fellowship Le 1341/1-1.



(a) Yell. (b) Red (c) Green (d) DullIR (e) Paper

**Figure 11:** Renderings (top row) and photos (bottom row) of different materials under UV light (400 nm).



(a) Yell. (b) Red (c) Green (d) DullIR (e) Paper

**Figure 12:** Renderings (top row) and photos (bottom row) of different materials under 5600K illumination.

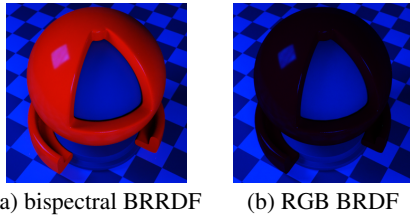


**Figure 13:** Measured fluorescent red bispectral BRRDF (a) compared to a simple RGB vector valued BRDF (b) under blue illumination. Note the cross-color reflectance from blue to red in the case of the full bispectral BRRDF. The RGB BRDF cannot represent these complex color shifts and fails to reproduce the fluorescent effect.

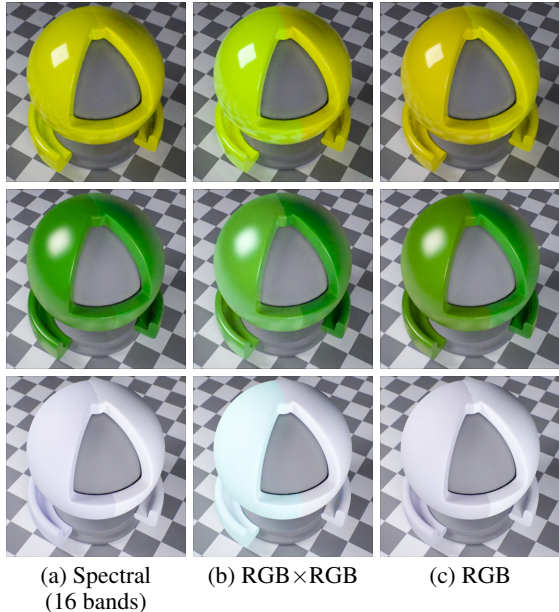


**Figure 14:** Comparison renderings using 3 different measured fluorescent materials. Full bispectral BRRDF measurements (right half of each sphere) are compared to: spectral measurements,  $RGB \times RGB$  reradiation matrices, and standard  $RGB$  BRDFs.

## References

- ANGELOPOULOU, E., AND MOLANA, R. 2001. Multispectral skin color modeling. In *IEEE Conference on Computer Vision and Pattern Recognition*, 635–642.
- BACCINI, A., BESSE, P., AND DE FALGUEROLLES, A. 1996. An L1-norm PCA and a heuristic approach. In *Ordinal and Symbolic Data Analysis*. Springer, 359–368.
- BENDIG, M., HANIKA, J., DAMMERTZ, H., GOLDSCHMIDT, J. C., PETERS, M., AND WEBER, M. 2008. Simulation of fluorescent concentrators. In *IEEE Symposium on Interactive Ray Tracing*, 93–98.
- CLARKE, F., AND PARRY, D. 1985. Helmholtz Reciprocity: its validity and application to reflectometry. *Lighting Research and Technology* 17, 1, 1–11.
- COOK, R., AND TORRANCE, K. 1981. A reflectance model for computer graphics. In *SIGGRAPH*, 307–316.
- CURET, 1996. Columbia Utrecht Texture Database. Web-Page. <http://www1.cs.columbia.edu/CAVE/software/curet/index.php>.
- DEROSE, P. C., EARLY, E. A., AND KRAMER, G. W. 2007. Qualification of a fluorescence spectrometer for measuring true fluorescence spectra. *Review of Scientific Instruments* 78.
- DONALDSON, R. 1954. Spectrophotometry of fluorescent pigments. *British Journal of Applied Physics* 5, 6, 210–214.
- GLASSNER, A. 1994. A Model for Fluorescence and Phosphorescence. In *Proc. of the Eurographics Workshop on Rendering*, 57–68.
- GUNDLACH, D., AND TERSTIEGE, H. 1994. Problems in measurement of fluorescent materials. *Color Research & Application* 19, 6, 427–436.
- HAVRAN, V., NEUMANN, A., ZOTTI, G., PURGATHOFER, W., AND SEIDEL, H.-P. 2005. On cross-validation and resampling of BRDF data measurements. In *SCCG '05: Proceedings of the 21st Spring Conference on Computer Graphics*, 161–168.
- HERSCH, R. D., DONZÉ, P., AND CHOSSON, S. 2007. Color images visible under UV light. *ACM Trans. Graph. (Proc. SIGGRAPH)* 26, 3, 75.
- HOLOPAINEN, S., MANOOCHERI, F., AND IKONEN, E. 2008. Goniofluorometer for characterization of fluorescent materials. *Applied Optics* 47, 6, 835–842.
- KAJIYA, J. 1986. The Rendering Equation. In *Computer Graphics (Proc. SIGGRAPH '86)*, 143–150.
- KE, Q., AND KANADE, T. 2003. Robust subspace computation using L1 norm. *Carnegie Mellon Tech Report CMU-CS-03-172*.
- LELAND, J. E., JOHNSON, N. L., AND ARECCHI, A. V. 1997. Principles of bispectral fluorescence colorimetry. *Photometric Engineering of Sources and Systems* 3140, 1, 76–87.
- MARSCHNER, S., WESTIN, S., LAFORTUNE, E., AND TORRANCE, K. 2000. Image-based bidirectional reflectance distribution function measurement. *Applied Optics* 39, 16, 2592–2600.
- MATUSIK, W., PFISTER, H., BRAND, M., AND McMILLAN, L. 2003. A data-driven reflectance model. *ACM Trans. Graph. (Proc. SIGGRAPH)* 22, 3, 759–769.
- MATUSIK, W., PFISTER, H., BRAND, M., AND McMILLAN, L. 2003. Efficient isotropic BRDF measurement. In *Proc. of the Eurographics Symposium on Rendering*, 241–248.
- NASSAU, K. 1983. *The Physics and Chemistry of Color: The Fifteen Causes of Color*. John Wiley and Sons, New York.
- NGAN, A., DURAND, F., AND MATUSIK, W. 2005. Experimental analysis of BRDF models. In *Proc. of the Eurographics Symposium on Rendering*, 117–226.
- NICODEMUS, F., RICHMOND, J., HSIA, J., GINSBERG, I., AND LIMPERIS, T. 1977. Geometrical considerations and nomenclature for reflectance. *National Bureau of Standards, Washington, DC. Inst. for Basic Standards*.
- PROCTOR, J., AND BARNES, Y. 1996. NIST high accuracy reference reflectometer-spectrophotometer. *Journal of Research of the Nat. Institute of Standards and Technology* 101, 5, 619–626.
- SPRINGSTEEN, A. 1999. Introduction to measurement of color of fluorescent materials. *Analyt. Chimica Acta* 380, 2–3, 183–192.
- WARD, G. J. 1992. Measuring and modeling anisotropic reflection. *Computer Graphics (Proc. SIGGRAPH)* 26, 2, 265–272.
- WILKIE, A., TOBLER, R., AND PURGATHOFER, W. 2001. Combined rendering of polarization and fluorescence effects. In *Proc. of the Eurographics Workshop on Rendering*, 197–204.
- WILKIE, A., WEIDLICH, A., LARBOULETTE, C., AND PURGATHOFER, W. 2006. A reflectance model for diffuse fluorescent surfaces. In *Proceedings of Graphite 2006*, 321–328.